Journal of Alloys and Compounds 831 (2020) 154784

Contents lists available at ScienceDirect

Journal of Alloys and Compounds

journal homepage: http://www.elsevier.com/locate/jalcom

Correlation among the amorphous forming ability, viscosity, free-energy difference and interfacial tension in Fe—Si—B—P soft magnetic alloys

Chengzhong Zhang [a, b], Qiang Chi [b], Jianhua Zhang [a, **], Yaqiang Dong [b], Aina He [b, *], Xiaoxiong Zhang [a], Pulong Geng [a], Jiawei Li [b], Huiyun Xiao [b], Jiancheng Song [a], Baolong Shen [c]

[a] National & Provincial Joint Engineering Laboratory of Mining Intelligent Electrical Apparatus Technology, College of Electrical and Power Engineering, Shanxi Key Laboratory of Coal Mining Equipment and Safety Control, Taiyuan University of Technology, No.79 Yingze West Avenue, Wanbolin District, Taiyuan, Shanxi, 030024, China

[b] CAS Key Laboratory of Magnetic Materials and Devices, Zhejiang Province Key Laboratory of Magnetic Materials and Application Technology, Ningbo Institute of Materials Technology and Engineering, Chinese Academy of Sciences, Ningbo, Zhejiang, 315201, China

[c] School of Materials Science and Engineering, Southeast University, Nanjing, 211189, China

ARTICLE INFO

Article history:
Received 14 January 2020
Received in revised form
9 March 2020
Accepted 13 March 2020
Available online 19 March 2020

Keywords:
Amorphous forming ability
Viscosity
Gibbs free-energy difference
Interfacial tension
Magnetic properties

ABSTRACT

To clarify the underlying mechanism of effects of P on amorphous forming ability (AFA) for Fe—Si—B—P alloy system, the AFA and melting viscosity of $(Fe_{76}Si_9B_{10})_{(100-x)/95}P_x$ (x = 0—3) amorphous alloys measured in the temperature range of 1200—1450 °C by oscillating cup method were investigated. A viscosity hysteresis occurs at about 1350 °C between the heating and cooling processes for all alloys, and the values of viscosity almost increase as P content increases at each measured temperature under cooling process. However, only considering viscosity cannot provide a satisfactory explanation for the trend of AFA for this alloy system. Afterwards, the mechanism was well revealed by calculating the Gibbs free-energy difference and speculating the interfacial tension. In addition, a positive correlation between magnetic properties (coercivity and effective permeability) and the AFA of this alloy system was also founded, which can provide an auxiliary in understanding the mechanism of AFA to some extent. Meanwhile, when x = 3, the alloy shows excellent soft magnetic properties including low coercivity of 0.9 A/m and high effective permeability of 17,000, which is promising for future electromagnetic device application.

1. Introduction

Amorphous forming ability (AFA) has been being a hotspot research topic and an unresolved issue since the Fe—P—C amorphous alloy was invented firstly by P. Duwez and his co-workers in 1967 [1]. In order to enhance the AFA and clarify its mechanism for Fe-based amorphous alloys, many efforts were devoted in the past decades. As a result, numerous Fe-based amorphous alloys including Fe—P—B [2], (Fe, Co, Ni)—Si—B [3], Fe-(Nb, Cr, Mo)-(Al, Ga)-(P, B, C) [4], Fe-(Cr, Mo)-(C, B)-Ln [5], and Fe—B—Si-M (M = Zr, Nb, Hf and Ta) [6], etc. were developed and the Fe—Si—B alloys (e.g. Metglas2605SA1) have been widely applied in industry [7]. However, the AFA of Fe-based amorphous alloys still remains at a low level. Especially for those commercialized alloys, the low AFA makes the thickness of corresponding ribbon less than 50 μm, leading to low packing density of transformer core, and hence increase in core loss [8]. Meanwhile, the AFA evaluations for Fe-based amorphous alloys are mostly based on some empirical indicators including reduced glass transition temperature (*Trg*), supercooled liquid region (ΔTx), γ and so on [9—13], which can be determined easily from differential thermal analysis (DTA) and differential scanning calorimetry (DSC). However, S. Mukherjee et al. [14], found that the *Trg* parameter was not always consistent with the experimental results. Moreover, Lu et al. [15], also pointed out that there is no one parameter or criterion that can provide a

* Corresponding author.
** Corresponding author.
E-mail addresses: zhangjianhua@tyut.edu.cn (J. Zhang), hean@nimte.ac.cn (A. He).

https://doi.org/10.1016/j.jallcom.2020.154784
0925-8388/

satisfactory explanation for the AFA of all bulk metallic glasses (BMGs), especially for Fe-based alloys with relatively low AFA, although they can supply some useful guidance in the development of BMGs. Therefore, continuous studies are still necessary in this field, for the preparation of most Fe-based amorphous alloys are performed in laboratory currently and the mechanism of AFA is also unclear.

As an essential factor to determine the AFA, the nucleation rate under solidification process [16], including driving force for crystallization, viscosity and interfacial tension between the nuclei and liquid phase, can be calculated thermodynamically and kinetically. The driving force for crystallization can be estimated by Gibbs free-energy difference between undercooled liquid and crystal. Unfortunately, the measurement of the interfacial tension can scarcely be achieved in experiments. Up to date, viscosities at high temperature of Fe-based amorphous-forming alloys were reported [17–22]. However, most of these studies focus much on the effect of ingredients on the viscosity itself, whilst the explicit relationship among AFA, viscosity, free-energy difference and interfacial tension of alloys have not been well discussed.

The metalloid element P plays an important role in the field of amorphous alloys. After many years of continued effort, many classic P-contained alloys systems, such as Pd-(Cu, Fe)–Ni–P, Fe–P–C and Fe–Si–B–P-(C) [23–28], were developed, which has provided an important groundwork for further research on the physical properties and mechanism of metallic glasses [29–32]. Up to date, besides as magnetic materials in electronic devices, the P-contained Fe-based amorphous alloys have made great progress in many other practical applications as catalysts [33,34], coatings [35,36], and dye wastewater treatment agents [37]. Furthermore, the P also has obvious effects in adjusting the AFA and magnetic properties of Fe-based amorphous alloys. For instance, substituting Si or Fe for P could promote AFA and magnetic properties of Fe–B–Si alloys [38,39]. However, the effects of P on AFA for the Fe-based amorphous alloys are still unclear.

In this paper, with the aim of clarifying the potential mechanism of effects of P on Fe–Si–B alloy system, the $(Fe_{76}Si_9B_{10})_{(100-x)/95}P_x$ alloy system was designed. The viscosity was measured using oscillating cup method over a large temperature range. Collaborating viscosity, free-energy difference and interfacial tension, the mechanism of the effect of P on the AFA of Fe–Si–B–P alloy system were revealed. Moreover, the magnetic properties have a close relationship with the AFA for an amorphous alloy [32,40]. Generally the change of AFA of one alloy will be reflected in its magnetic properties [41]. Therefore, in this paper the magnetic properties also were investigated to provide auxiliary to better explain the AFA of this alloy system.

2. Experimental procedures

The master alloys with a nominal composition of $(Fe_{76}Si_9B_{10})_{(100-x)/95}P_x$ ($x = 0–3$) were prepared by arc-melting the mixture of pure Fe (99.97 wt%), Si (99.999 wt%), pre-alloy of Fe-23.31%P, and Fe-17.64%B in purified Argon atmosphere. The alloys were renamed according to the P content as alloy P0 ($x = 0$) to alloy P3 ($x = 3$). The AFA was assessed by the critical wheel speed (v_{cr}) of producing fully amorphous ribbons with width of about 0.9 mm prepared by using single-roller melt-spinning method. The wheel speed changes with a step of 5 m/s.

The phase identification of the as-cast ribbons with different thickness was carried out by using an X-ray diffractormeter (XRD) with Cu *Kα* radiation. The thermal properties associated with crystallization temperature (T_x) and the Curie temperature (T_c) were measured by DSC at a constant heating rate of 0.67 °C/s. Melting (T_m) and liquidus (T_l) temperatures were characterized by DTA at rate of 0.67 and 0.067 °C/s, respectively.

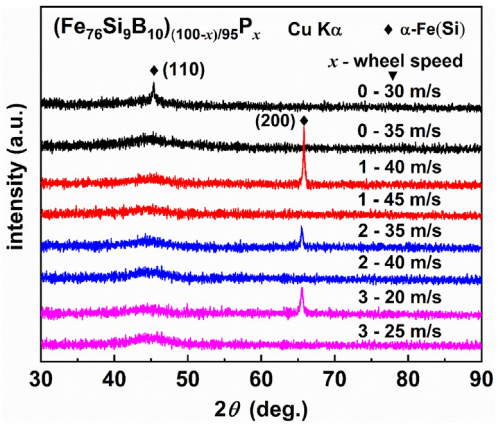

Fig. 1. XRD patterns of the $(Fe_{76}Si_9B_{10})_{(100-x)/95}P_x$ ($x = 0$, 1, 2 and 3) as-spun alloy ribbons prepared at different wheel speed.

High temperature viscosity was measured by the oscillating cup method corresponding measuring procedures and principles have been described in detail in Ref. [42]. The samples with a mass of about 140 g were put into a heat-resistant alundum crucible contained in a graphite vessel that was hung in a torsional suspension chamber. To avoid oxidation at high temperature, the furnace chamber was filled up with Argon after evacuating to a pressure of 10^{-3} Pa. All experiments were carried out in Argon with a constant temperature interval of 50 °C from 1200 to 1450 °C upon heating and cooling at a rate of 0.167 °C/s. In order to obtain a homogeneous melt, the sample was held for 30 min under isothermal conditions at each targeted temperature before measurements. The viscosity was measured at least three times at each temperature and the average value was used.

The saturation magnetic induction (B_s), coercivity (H_c) and effective permeability (μ_e) were measured with a vibrating sample magnetometer (VSM) under an applied field of 800 kA/m, a B–H loop tracer under a field of 800 A/m and an impedance analyzer under a field of 1 A/m, respectively. The density of all samples was measured using the Archimedean method. All the measurements were performed at room temperature.

All the experiments in this work, such as viscosity, magnetic properties, DSC and DTA curves, have been repeated three times and at least three samples were prepared for each measurement, such as magnetic properties, DSC and DTA curves, in order to ensure the repeatability.

3. Results

The AFA of alloys is closely related to the composition, and can be evaluated by the critical cooling rate (minimum wheel speed, v_{cr}) of preparing fully amorphous ribbons confirmed by XRD. The corresponding patterns of as-spun ribbons prepared at different wheel speeds are shown in Fig. 1. For alloy P0, when the wheel speed is 30 m/s, a sharp peak superimposed on the amorphous halo at about $2\theta = 45°$, relating to the reflection of (110) plane of α-Fe (Si) crystalline phase, can be identified. With the speed increasing to 35 m/s, only one broad peak and no evident sharp peak can be observed for this alloy, indicating its fully amorphous structure. The ribbons prepared with speed of 40 m/s, 35 m/s and 20 m/s are partially amorphous due to the sharp peaks occurring at about $2\theta = 65°$ identified as a (200) crystal plane of α-Fe (Si) phase for the alloy P1, P2 nd P3, respectively. At the same time, these peaks vanish when the wheel speed increases to 45 m/s, 40 m/s and 25 m/

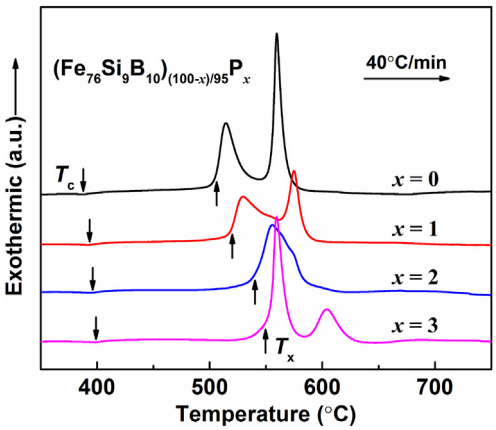

Fig. 2. DSC curves of melt-spun $(Fe_{76}Si_9B_{10})_{(100-x)/95}P_x$ (x = 0, 1, 2 and 3) amorphous alloys.

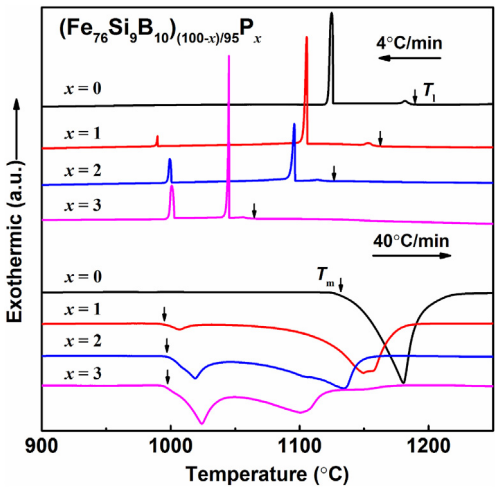

Fig. 3. DSC and DTA curves of $(Fe_{76}Si_9B_{10})_{(100-x)/95}P_x$ (x = 0, 1, 2 and 3) alloys upon melting and solidification processes.

s, respectively. Here, it is worth noticing a peculiar phenomenon which the sharp peaks appear at different position for P0 alloy and others. This phenomenon is closely related to the crystalline texture. As is well known, the segregation of P element can easily occur in Fe–P alloys and is an important factor controlling the variation of orientation during the crystallization [43]. For the P0 alloy, its α-Fe (Si) phase have a random orientation. After the doping of P, the (110)-plane in the precipitated α-Fe (Si) phase changed to preferred orientation (200)-plane which parallels to the ribbon surface. The similar result also was reported in the $Fe_{84.3}Cu_{0.7}Si_4B_8P_3$ alloy [44]. According to these results, it can be noticed that the AFA of Fe–Si–B alloys dose not present monotonically enhanced tendency with the P addition.

Fig. 2 shows the DSC traces of as-spun amorphous ribbons of this alloy system. As is shown in Fig. 2, the T_c slightly increases from 387.9 to 397.7 °C with the P content rising. This results can be explained by the Bethe–Slater curve. According to this curve, especially when the content of metalloid elements in Fe-based alloys is no more than 25 at.%, as the Fe content decreases, the atomic spacing would increase and the magnetic exchange interaction between Fe atoms will be strengthen, leading to the increasing of T_c [27,45]. Hence, in this experiment, the T_c increased with the P doping and the decreasing of the Fe content. All the amorphous ribbons exhibit directly crystallization behavior without observing any glass transition temperature T_g, meaning the parameters associated with T_g cannot be obtained. The T_x shifts to higher temperature with the increase of P content. For the crystallization stage, according to the literatures [46–48], the first and second exothermic peaks relate to the primary crystallization of α-Fe (Si) grains and the precipitation of Fe–B compounds, respectively. It can be also found the temperature interval between T_x and T_c increases from 116.8 to 146.5 °C, which is beneficial to widen annealing temperature window and release stress completely in industrial annealing process. Fig. 3 exhibits the DSC and DTA curves of the investigated amorphous alloys during melting and solidification processes. The corresponding results of T_m and T_l for all investigated alloys are listed in Table 1. Here, it is found that the T_m drastically reduces from 1149 to 995.1 °C with addition of 1 at.% P and subsequently increases slowly to 1005.7 °C as the P content further increases to 3 at.%. This phenomenon can be explained by the binary phase diagrams of Fe–Si, Fe–B, and Fe–P alloys [49]. In this diagram, the liquidus temperatures for the Fe–P alloy exhibit a descent tendency as the content of P element increases, which basically accords with the Fe–B alloy but higher than that of Fe–Si when the single metalloid element (B, P and Si) content is lower than 7.5 at.%. According to the diagram, certainly, the T_m will decrease firstly with the P content varying from 0 to 1 at.%. Subsequently, as the content of P further increases from 1 to 3 at.%, the content of Si and B in the alloy will decrease accordingly, and the T_m will surely increase slightly again. Moreover, the mixing entropy of Fe–P is −31 kJ/mol transcending that of Fe–B (-11 kJ/mol) and Fe–Si (−18 kJ/mol) [27,49], making the numbers of Fe–P compounds increase as the P content rises. Therefore, the T_m decreases and then increases with increasing the P content. Meanwhile, the T_l gradually reduces from 1186.3 for the alloy P0 to 1059.6 °C for the alloy P3. These changes indicate that the alloy gradually approaches a eutectic point with an increase of P content from 0 to 3 at.%.

It is widely accepted that the viscosity determines the nucleation process and governs the AFA of an alloy to a large extent [50]. Therefore, viscosity is systematically studied here to clarify the reasons for P affecting the AFA of the Fe–B–Si alloy. Fig. 4 shows the temperature dependence of viscosity for the $(Fe_{76}Si_9B_{10})_{(100-x)/95}P_x$ (x = 0, 1, 2 and 3) alloy melts during heating and cooling processes. The values of viscosity for all the alloy melts over the measured temperature interval are less than 14 mPa s, which is consistent with the magnitude reported in Fe–Si–B–P–C alloys [22]. From Fig. 4, a monotonic decrease trend of viscosity can be observed for each alloy melt with the increasing of temperature. There is a sharply decrease for each sample when the temperature is near to 1350 °C. This abnormal temperature is usually named as dissolution temperature T_{dis} [51]. Meanwhile, a hysteresis of viscosity for all melting alloys also is observed after all samples heated to 1450 °C, and then cooled (the viscosity values, measured in cooling process are lower than those obtained upon heating process). For alloy P0, the hysteresis maintains even the temperature is 1200 °C, which accords with the result reported in $Fe_{80}B_{14}Si_6$ melt [18]. For alloys P1 and P2, the viscosity curves are relatively smooth, and overlap again when the temperature is near to 1250 °C. Cooled below 1300 °C, an evident increase of viscosity is observed for the P3 alloy melt.

In fact, viscosity is an essential reflection of the evolution of the melt structure. Hence, the viscosity anomalies can be explained from aspects of clusters and structural transformation. According to Dong et al. [52,53], many kinds of clusters, including Fe–B, Fe–Si, Fe–P and pure Fe, exist in Fe–Si–B–P alloy systems, and the types, structure and number of cluster vary accordingly with the variation of composition and temperature. In the heating process, owing to the heating rate and thermal relaxation, the types, structure and

Table 1
The AFA (critical wheel speeds), thermodynamic parameters, and magnetic properties of P0, P1, P2 and P3 amorphous alloys.

Alloy	AFA (v_{cr}, m/s)	T_{x1} (°C)	T_m (°C)	T_l (°C)	ΔH_l (kJ/mol)	ΔG_{l-x} (kJ/mol)	μ_e (1 kHz)	H_c (A/m)
P0	35	504.7	1149	1186.3	12.99	2.59	10,200	1.7
P1	45	517.8	995.1	1157.6	11.41	2.28	8300	1.9
P2	40	539.5	999.8	1119.0	10.40	2.08	9200	1.5
P3	25	544.2	1005.7	1059.6	10.31	2.06	17,000	0.9

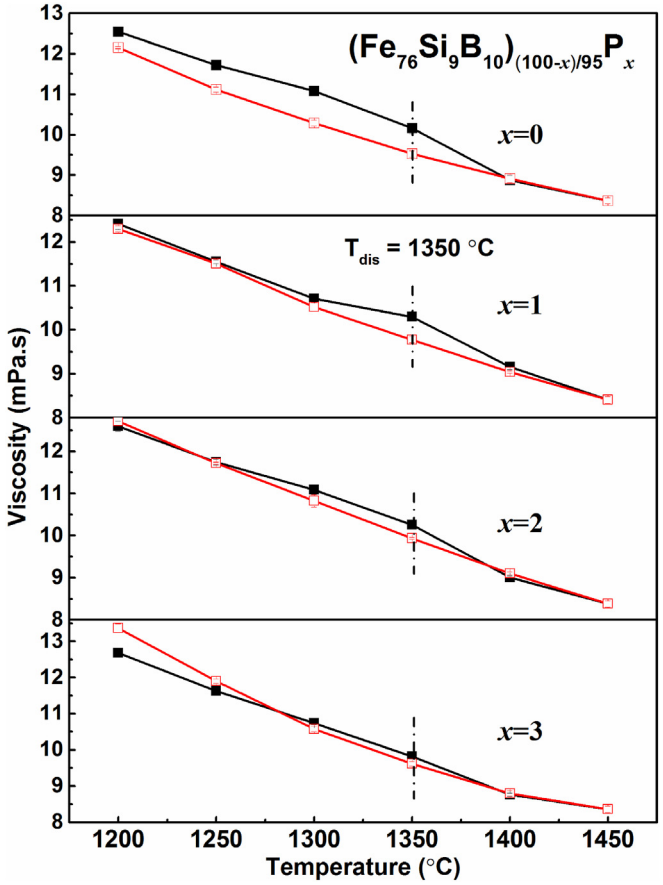

Fig. 4. Temperature dependence of viscosity for the $(Fe_{76}Si_9B_{10})_{(100-x)/95}P_x$ (x = 0, 1, 2 and 3) alloy melts during heating (■) and cooling processes (□).

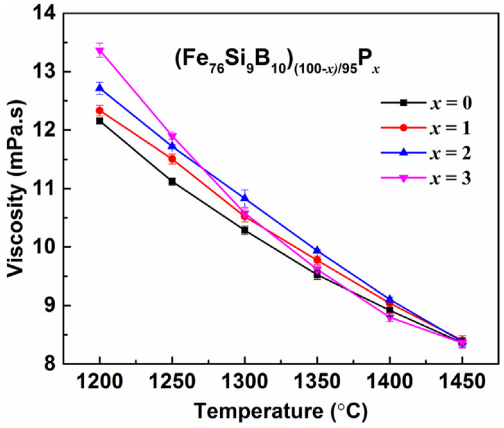

Fig. 5. The temperature dependence of viscosity for the $(Fe_{76}Si_9B_{10})_{(100-x)/95}P_x$ (x = 0, 1, 2 and 3) alloy melts during cooling process.

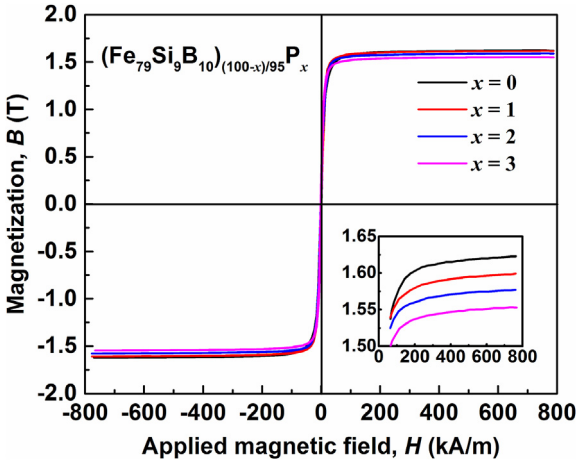

Fig. 6. Hysteresis B–H loops of $(Fe_{76}Si_9B_{10})_{(100-x)/95}P_x$ (x = 0, 1, 2 and 3) amorphous ribbons. Inset is the enlarged view of part of the hysteresis B–H loops.

number of cluster existing in the melts may remain a relative thermodynamic equilibrium state before the temperature is above T_{dis}. Around T_{dis}, the atomic bonds in these clusters will be destroyed dramatically and the movement of the atoms will be more fast, leading to a large decrease of viscosity in the subsequent short heating period. Conversely, during the cooling process, the thermodynamic equilibrium state would maintain over a larger temperature range before a sudden increase in viscosity. Consequently, the existing clusters, their structural transformation as well as the thermal relaxation will lead to the result that the viscosity values measured in cooling process are lower than those obtained upon heating process and the formation of viscosity hysteresis [18]. While the trend of viscosity can be generally attributed to the composition change, the relation of viscosity between heating and cooling processes, involving the member, types and superfine structure of clusters, will be more complicated and need further study.

Here, the viscosity under cooling process for this alloy system is mainly considered, for the amorphous alloy was prepared by adopting a rapid solidification technology. In Fig. 5, the corresponding data in cooling process are illustrated together to facilitate the comparison and understand the mechanism of P on the AFA for this alloy system. It is obvious that the viscosity of each melt almost has a same value at the 1450 °C, and presents an increase trend with the decreasing temperature. At same temperature, as the P content increases from 0 to 2 at.%, the viscosity shows an evidently increase. However, for alloy P3, the viscosity has a lower values compared with that of other alloys over the temperature range of 1450 to 1350 °C, and subsequently displays a rapid increase when the temperature is below 1300 °C. Overall, the higher the P content, the higher viscosity values for this alloy system at low temperature range, especially when the temperature is below 1250 °C, which is consistent with the trend of T_l.

The magnetic properties (B_s, H_c and μ_e) for this alloy system are shown in Figs. 6 and 7. All ribbon samples for magnetic properties measurements have annealed for 10 min at the temperatures of T_x

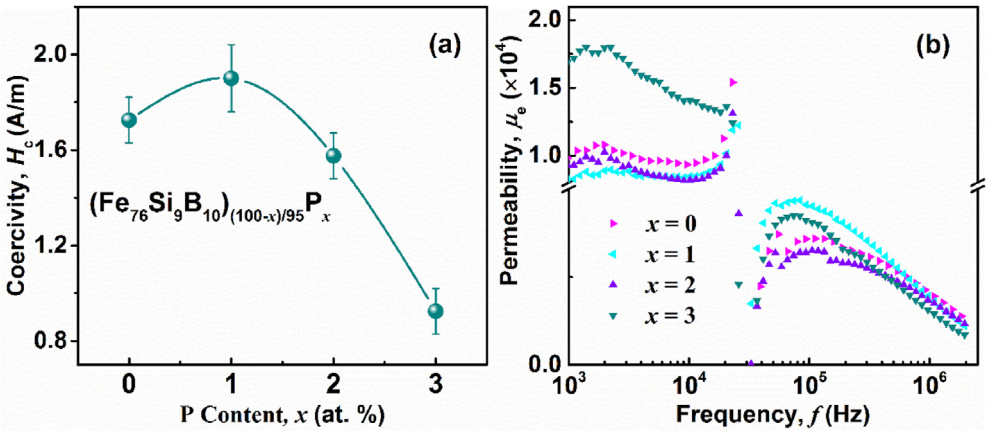

Fig. 7. The coercivity (a) and effective permeability as a function of applied field frequency (b) of $(Fe_{76}Si_9B_{10})_{(100-x)/95}P_x$ ($x = 0$, 1, 2 and 3) amorphous ribbons annealed for 10 min at the temperature of $T_{x1} - 90$ °C.

$-$ 90 °C by using isothermal furnace under a low pressure of about 5×10^{-3} Pa to release internal stress. During this stage the defects like free volume can be eliminated, which results in a more uniform microstructure and hence optimizes magnetic performance. As is shown in Fig. 6, the B_s are 1.62, 1.60, 1.57 and 1.55 T for P0, P1, P2 and P3 annealed ribbons, respectively. It is clear that the B_s presents a monotonically decreasing trend as the increase of P content, which is attributed to the reducing of Fe content. Meanwhile, The H_c showed in Fig. 7(a) increases at first and then decreases as P content elevates, and the alloy P3 has the lowest value of 0.9 A/m. The frequency dependence of μ_e under a field of 1 A/m for this alloy system is shown in Fig. 7(b). It can been found from Fig. 7(b) that the μ_e of alloy samples exhibit a similar change tendency compared to the H_c. And the alloy P3 presents a high value of 17,000 at 1 kHz, which is much higher than that of other Fe-based amorphous alloys [54–56]. The magnetic properties and AFA of all alloys are also summarized in Table 1, which will be discussed more detail below.

4. Discussion

The thermal properties of this alloy system are studied at first to explore the mechanism of AFA under the experimental results in Fig. 1. However, there is no distinct glass transition can be observed for all samples, so the parameters associated with T_g cannot be calculated. According to the previous literatures [10,57], it seems that the compositions of alloys with good AFA are at or very close to the eutectic point. Currently, the widely accepted theory is that when the alloy composition is close to the eutectic point, a variety of crystal phases will be competing for precipitation and viscosity of the alloy will increase exponentially with decreasing temperature. Therefore, the atomic rearrangement becomes more difficult during the cooling process, which is advantageous for the formation of amorphous state [57]. However, this cannot perfectly explain why the alloy P0 has the highest T_l compared with alloy P1 and P2 simultaneously possesses the best AFA.

From the discussion above, it can be found that the thermodynamic parameters obtained from DSC and DTA curves cannot well explain the effect of P on the AFA of Fe–Si–B alloy system and other factors should be taken into consideration. According to Turnbull, the typical nucleation rate I_v can be expressed as [58]:

$$Iv(T) = \frac{Av}{\eta(T)} \exp\left(\frac{-16\pi\left(\sigma^{l-x}\right)^3}{3kT\left(\Delta G^{l-x}(T)\right)^2}\right) \quad (1)$$

where Av is a constant, k the Boltzmann's constant, T the absolute temperature, σ^{l-x} the interfacial tension between the liquid and crystalline, $\eta(T)$ the temperature dependence viscosity, and ΔG^{l-x} the free-energy difference between the liquid and crystal.

In terms of the viscosity $\eta(T)$, according to Eq. (1), it is evident that a higher value or a rapid drops of viscosity with decreasing temperature will lead to a lower nucleation rate, which is beneficial to the AFA. As illustrated in Fig. 5, the values of viscosity in cooling processes exhibit a rising trend with the increasing of P content. Meanwhile, the AFA also enhances progressively for alloy P1, P2 and P3, which accords well with the trend of viscosity. However, the special phenomenon that alloy P0 exhibits lowest viscosity and better AFA compared with that of alloys P1 and P2 cannot be explained by only viscosity.

The free-energy difference ΔG^{l-x} can be calculated by using an approximate method. After taking into account the Turnbull's approximation, the difference of the specific heat capacity (Δc_p^{l-x}) between the liquid and crystal will equal to 0 for the temperature below T_l, and free-energy difference can be estimated through the formula proposed by Alexander et al. [59], which can be expressed as:

$$\Delta G^{l-x} \cong -\frac{\Delta H_l}{T_l}\Delta T \quad (2)$$

where ΔH_l is the enthalpy of fusion, ΔT the undercooling degree and T_l the liquids temperature. These parameters are detailed listed in Table 1. The ΔG^{l-x} are 2.59, 2.28, 2.08 and 2.06 kJ/mol for P0, P1, P2 and P3 alloys, respectively. A smaller ΔG^{l-x} leads to a lower nuclei according to Eq. (2). From this point of view, the AFA of this alloy system should be gradually improved with the P content increasing, which does not completely agree with the experimental results.

It is worth noting here that in addition to viscosity and free-energy difference, the interfacial tension between the liquid and crystal also plays an important role in the nucleation rate. Particularly, the nucleation rate is more sensitive to interfacial tension compared with free-energy difference and viscosity, because the interfacial tension has a cubic dependence on interfacial tension [60]. A higher interfacial tension is beneficial for the suppression of the nucleation process, whereas the interfacial tension is barely measured experimentally. Fortunately, the effect of P on the surface tension of FeSiBPC alloys have been reported by Dong et al. [61]. This study indicated that the surface tension presents a decrease trend with increasing P content. The P element is a surface active element, which can weaken the interaction between the liquid and

clusters in melt, leading to a lower surface tension. Hence, it can be speculated here that, in the Fe−Si−B alloy systems, the surface tension will decrease with the addition of P element. For P element will aggregates into the surface layer of the liquid, which weakens the interaction between the liquid and the solid phase, the interfacial tension would also decrease.

Hence, although alloy P0 shows the lowest value of viscosity and highest free-energy difference, the AFA of the P0 alloy is better than that of the P1 and P2 alloys as it possesses the highest interfacial tension among all the alloys, which has a greater influence on the nucleation rate. The phenomenon the AFA again gradually rise with the P content further increases from 1 to 3 at.% can be attributed to that the viscosity and free-energy difference together show much greater influence than interfacial tension on the nucleation rate.

In addition, it has been proved that the microstructure and quality of amorphous products have a significant effect on their magnetic properties. Therefore, in this work, the magnetic properties also be studied systematically to verify the change of AFA in this alloy system. According to Fig. 7 and Table 1, it is surprised that the variation of magnetic parameters are well consistent with the trend of AFA for these alloys, and the lowest H_c and highest μ_e are corresponding to the highest AFA. This phenomenon can be well interpreted by the changes of AFA. In general, an alloy with better AFA also possesses a more uniform microstructure and less free volume, resulting in less number of magnetic domain pinning sites, smaller magnetic anisotropy and hence a lower H_c and higher μ_e. Moreover, The μ_e for the alloy P3 have high value of about 14,000 at 10 kHz, which are useful in a variety of high-frequency application such as high-frequency transformer cores.

5. Conclusions

In summary, the effect of P content on the AFA of $(Fe_{76}Si_9B_{10})_{(100-x)/95}P_x$ alloys has been investigated in this work. In this alloy system, the viscosity presents an increase tendency upon the cooling process with the P content rising. The free-energy difference and the interfacial tension speculated based on previous studies gradually decreases with increasing the P content. Finally, the change of AFA and the underlying mechanism for this alloy system are explained thermodynamically and kinetically by collaborating the viscosity, free-energy difference and interfacial tension. In addition, The change of H_c and μ_e are also consistent with the AFA, and the relationship between magnetic properties and the AFA of this alloy system are verified.

Declaration of competing interest

The authors declared that they have no conflicts of interest to this work. We declare that we do not have any commercial or associative interest that represents a conflict of interest in connection with the work submitted.

CRediT authorship contribution statement

Chengzhong Zhang: Conceptualization, Investigation, Methodology, Software, Writing - original draft, Validation. **Qiang Chi:** Conceptualization, Data curation, Software. **Jianhua Zhang:** Data curation, Writing - review & editing, Conceptualization, Funding acquisition. **Yaqiang Dong:** Data curation, Methodology. **Aina He:** Data curation, Writing - review & editing, Conceptualization, Funding acquisition. **Xiaoxiong Zhang:** Investigation. **Pulong Geng:** Methodology, Formal analysis. **Jiawei Li:** Data curation, Methodology. **Huiyun Xiao:** Formal analysis. **Jiancheng Song:** Methodology, Project administration, Resources. **Baolong Shen:** Methodology, Supervision.

Acknowledgements

This work was supported by the National Key Research and Development Program of China (Grant No. 2016YFB0300500), the National Natural Science Foundation of China (Grant No. 51701136, 51801224 and 51771083), the Zhejiang Provincial Natural Science Foundation (Grant No. LQ18E010006), the Shanxi Provincial Natural Science Foundation (Grant No. 201901D211044 and 201803D121024).

References

[1] P. Duwez, S.C.H. Lin, Amorphous ferromagnetic phase in iron-carbon-phosphorus alloys, J. Appl. Phys. 38 (1967) 4096−4097.
[2] K. Yamauchi, Y. Nakagawa, Amorphous ferromagnetic Fe-P-B alloys prepared by a new technique of splat cooling, Jap. J. Appl. Phys. 10 (1971) 1730.
[3] M. Kikuchi, H. Fujimori, Y. Obi, T. Masumoto, New amorphous ferromagnets with low coercive force, Jap. J. Appl. Phys. 14 (1975) 1077−1078.
[4] A. Inoue, J.S. Gook, Effect of additional elements (M) on the thermal stability of supercooled liquid in $Fe_{72-x}Al_5Ga_2P_{11}C_6B_4M_x$ glassy alloys, Mater T Jim 37 (1996) 32−38.
[5] V. Ponnambalam, S.J. Poon, G.J. Shiflet, Fe-based bulk metallic glasses with diameter thickness larger than one centimeter, J. Mater. Res. 19 (2004) 1320−1323.
[6] Y.X. Geng, X. Lin, J. Li, S.M. Fan, H.B. Ju, L.H. Yu, J.H. Xu, Y.M. Wang, Super-high hardness of (Fe,Co)-B-Si-Zr/Hf bulk glassy alloys, J. Alloys Compd. 753 (2018) 351−355.
[7] R.B. Frédéric Mazaleyrat, Chapter 3−Soft amorphous and nanocrystalline magnetic materials, in: H.S. Nalwa (Ed.), Handbook of Advanced Electronic and Photonic Materials and Devices, vol. 6, Elsevier Inc. Academic press, 2001, pp. 59−102.
[8] R.B. Schwarz, T.D. Shen, U. Harms, T. Lillo, Soft ferromagnetism in amorphous and nanocrystalline alloys, J. Magn. Magn Mater. 283 (2004) 223−230.
[9] Z.P. Lu, C.T. Liu, W.D. Porter, Role of yttrium in glass formation of Fe-based bulk metallic glasses, Appl. Phys. Lett. 83 (2003) 2581−2583.
[10] C. Suryanarayana, A. Inoue, Iron-based bulk metallic glasses, Int. Mater. Rev. 58 (2013) 131−166.
[11] A. Inoue, B.L. Shen, C.T. Chang, Fe- and Co-based bulk glassy alloys with ultrahigh strength of over 4000 MPa, Intermetallics 14 (2006) 936−944.
[12] D.S. Song, J.H. Kim, E. Fleury, W.T. Kim, D.H. Kim, Synthesis of ferromagnetic Fe-based bulk glassy alloys in the Fe-Nb-B-Y system, J. Alloys Compd. 389 (2005) 159−164.
[13] W. Zhang, H.T. Miao, Y.H. Li, C.T. Chang, G.Q. Xie, X.J. Jia, Glass-forming ability and thermoplastic formability of ferromagnetic $(Fe, Co, Ni)_{75}P_{10}C_{10}B_5$ metallic glasses, J. Alloys Compd. 707 (2017) 57−62.
[14] S. Mukherjee, J. Schroers, Z. Zhou, W.L. Johnson, W.K. Rhim, Viscosity and specific volume of bulk metallic glass-forming alloys and their correlation with glass forming ability, Acta Mater. 52 (2004) 3689−3695.
[15] H.X. Li, Z.C. Lu, S.L. Wang, Y. Wu, Z.P. Lu, Fe-based bulk metallic glasses: glass formation, fabrication, properties and applications, Prog. Mater. Sci. 103 (2019) 235−318.
[16] W.H. Wang, C. Dong, C.H. Shek, Bulk metallic glasses, Math. Sci. Eng. R. 44 (2004) 45−89.
[17] A.L. Bel'tyukov, V.I. Lad'yanov, A.I. Shishmarin, S.G. Menshikova, Viscosity of liquid amorphizing alloys of iron with boron and silicon, J. Non-Cryst. Solids 401 (2014) 245−249.
[18] V.I. Lad'yanov, A.L. Bel'tyukov, V.V. Maslov, A.I. Shishmarin, M.G. Vasin, V.K. Nosenko, V.A. Mashira, Viscosity of glass forming alloys based on Fe-Si-B system, J. Non-Cryst. Solids 353 (2007) 3264−3268.
[19] M. Tomut, H. Chiriac, Viscosity and surface tension of liquid Fe-metalloid glass-forming alloys, Mat. Sci. Eng. A-Struct. 304 (2001) 272−276.
[20] R. Parthiban, M. Stoica, I. Kaban, R. Kumar, J. Eckert, Viscosity and fragility of the supercooled liquids and melts from the Fe-Co-B-Si-Nb and Fe-Mo-P-C-B-Si glass-forming alloy systems, Intermetallics 66 (2015) 48−55.
[21] T. Yamasaki, N. Yufune, H. Ushio, D. Okai, T. Fukami, H.M. Kimura, A. Inoue, Viscosity measurements for Fe-Ni-B and Fe-Ni-Al-B liquid alloys by an oscillating crucible method, Mat. Sci. Eng. A-Struct. 375 (2004) 705−708.
[22] Y. Li, W.-z. Chen, B.-s. Dong, S.-x. Zhou, Effects of metalloid content on viscosity of Fe-Si-B-P-C alloy melt, J. Non-Cryst. Solids 490 (2018) 31−34.
[23] T.D. Shen, Y. He, R.B. Schwarz, Bulk amorphous Pd-Ni-Fe-P alloys: preparation and characterization, J. Mater. Res. 14 (1999) 2107−2115.
[24] O. Gross, S.S. Riegler, M. Stolpe, B. Bochtler, A. Kuball, S. Hechler, R. Busch, I. Gallino, On the high glass-forming ability of Pt-Cu-Ni/Co-P-based liquids, Acta Mater. 141 (2017) 109−119.
[25] A. Makino, C.T. Chang, T. Kubota, A. Inoue, Soft magnetic Fe-Si-B-P-C bulk metallic glasses without any glass-forming metal elements, J. Alloys Compd. 483 (2009) 616−619.
[26] J.F. Wang, R. Li, N.B. Hua, L. Huang, T. Zhang, Ternary Fe-P-C bulk metallic glass with good soft-magnetic and mechanical properties, Scripta Mater. 65 (2011) 536−539.
[27] J.H. Zhang, C.T. Chang, A.D. Wang, B.L. Shen, Development of quaternary Fe-

based bulk metallic glasses with high saturation magnetization above 1.6 T, J. Non-Cryst. Solids 358 (2012) 1443–1446.
[28] T.D. Shen, R.B. Schwarz, Bulk ferromagnetic glasses in the Fe-Ni-P-B system, Acta Mater. 49 (2001) 837–847.
[29] A. Makino, X. Li, K. Yubuta, C.T. Chang, T. Kubota, A. Inoue, The effect of Cu on the plasticity of Fe-Si-B-P-based bulk metallic glass, Scripta Mater. 60 (2009) 277–280.
[30] S. Hosokawa, H. Sato, N. Happo, K. Mimura, Y. Tezuka, T. Ichitsubo, E. Matsubara, N. Nishiyama, Electronic structure of $N_{42.5}N_{7.5}Cu_{30}P_{20}$, an excellent bulk metallic glass former: comparison to the $Pd_{40}Ni_{40}P_{20}$ reference glass, Acta Mater. 55 (2007) 3413–3419.
[31] A. Griesche, M.P. Macht, J.P. Garandet, G. Frohberg, Diffusion and viscosity in molten $Pd_{40}Ni_{40}P_{20}$ and $Pd_{40}Cu_{30}Ni_{10}P_{20}$ alloys, J. Non-Cryst. Solids 336 (2004) 173–178.
[32] A. Makino, T. Kubota, C.T. Chang, M. Makabe, A. Inoue, FeSiBP bulk metallic glasses with high magnetization and excellent magnetic softness, J. Magn. Magn Mater. 320 (2008) 2499–2503.
[33] Z. Jia, Q. Wang, L.G. Sun, Q. Wang, L.C. Zhang, G. Wu, J.H. Luan, Z.B. Jiao, A.D. Wang, S.X. Liang, M. Gu, J. Lu, Attractive in situ self-reconstructed hierarchical gradient structure of metallic glass for high efficiency and remarkable stability in catalytic performance, Adv. Funct. Mater. 29 (2019) 1807857.
[34] L.C. Zhang, Z. Jia, F. Lyu, S.X. Liang, J. Lu, A review of catalytic performance of metallic glasses in wastewater treatment: recent progress and prospects, Prog. Mater. Sci. 105 (2019) 100576.
[35] S.J. Pang, T. Zhang, K. Asami, A. Inoue, Synthesis of Fe–Cr–Mo–C–B–P bulk metallic glasses with high corrosion resistance, Acta Mater. 50 (2002) 489–497.
[36] J.B. Cheng, Q. Liu, B. Sun, X.B. Liang, B.S. Zhang, Structural and tribological characteristics of nanoscale FePSiBNb coatings, J. Therm. Spray Technol. 26 (2016) 530–538.
[37] Q.Q. Wang, M.X. Chen, L.L. Shao, Y.W. Ge, P.H. Lin, C.L. Chu, B.L. Shen, Effects of structural relaxation on the dye degradation ability of FePC amorphous alloys, J. Non-Cryst. Solids 525 (2019) 119671.
[38] C.J. Wang, A.N. He, A.D. Wang, J. Pang, X.L. Liang, Q.F. Li, C.T. Chang, K.Q. Qiu, X.M. Wang, Effect of P on glass forming ability, magnetic properties and oxidation behavior of FeSiBP amorphous alloys, Intermetallics 84 (2017) 142–147.
[39] H. Gao, R. Xiang, S.X. Zhou, B.S. Dong, Y.G. Wang, The influence of P on glass forming ability and clusters in melt of FeSiBP amorphous soft-magnetic alloy, J. Mater. Sci. Mater. Electron. 26 (2015) 7804–7810.
[40] J.J. Si, C.X. Du, T. Wang, Y.D. Wu, R.S. Wang, X.D. Hui, Glass formation and soft magnetic properties of novel Fe-rich Fe-B-Ti-Zr bulk metallic glasses, J. Alloys Compd. 741 (2018) 542–548.
[41] B.L. Shen, A. Inoue, Bulk glassy Fe-Ga-P-C-B-Si alloys with high glass-forming ability, high saturation magnetization and good soft magnetic properties, Mater. Trans. 43 (2002) 1235–1239.
[42] S.I. Bakhtiyarov, R.A. Overfelt, Measurement of liquid metal viscosity by rotational technique, Acta Mater. 47 (1999) 4311–4319.
[43] L. Zhang, L. Xiong, H. Ning, D. Ye, B.J. Duggan, Influence of segregation of phosphorus on texture development in cold-rolled Fe-P alloys during annealing, Mater. Sci. Forum 157–162 (1994) 1513–1522.
[44] E. Lopatina, I. Soldatov, V. Budinsky, M. Marsilius, L. Schultz, G. Herzer, R. Schäfer, Surface crystallization and magnetic properties of $Fe_{84.3}Cu_{0.7}Si_4B_8P_3$ soft magnetic ribbons, Acta Mater. 96 (2015) 10–17.
[45] K. Narita, J. Yamasaki, H. Fukunaga, Composition dependence of magnetic-moment and curie-temperature in amorphous $(Fe_xCo_{100-x})_{100-(y+z)}Si_yB_z$ ribbons, IEEE Trans. Magn. 14 (1978) 1016–1018.
[46] J. Xu, Y.Z. Yang, W. Li, Z.W. Xie, X.C. Chen, Effect of Si addition on crystallization behavior, thermal ability and magnetic properties in high Fe content Fe-Si-B-P-Cu-C alloy, Mater. Res. Bull. 97 (2018) 452–456.
[47] Y.M. Chen, T. Ohkubo, M. Ohta, Y. Yoshizawa, K. Hono, Three-dimensional atom probe study of Fe–B-based nanocrystalline soft magnetic materials, Acta Mater. 57 (2009) 4463–4472.
[48] X.F. Miao, Y.G. Wang, M. Guo, Structural, thermal and magnetic properties of Fe-Si-B-P-Cu melt-spun ribbons: application of non-isothermal kinetics and the amorphous random anisotropy model, J. Alloys Compd. 509 (2011) 2789–2792.
[49] A.D. Wang, C.L. Zhao, A.N. He, H. Men, C.T. Chang, X.M. Wang, Composition design of high B-s Fe-based amorphous alloys with good amorphous-forming ability, J. Alloys Compd. 656 (2016) 729–734.
[50] H.J. Zheng, L.N. Hu, X. Zhao, C.Z. Wang, Q.J. Sun, T. Wang, X.D. Hui, Y.Z. Yue, X.F. Bian, Poor glass-forming ability of Fe-based alloys: its origin in high-temperature melt dynamics, J. Non-Cryst. Solids 471 (2017) 120–127.
[51] U. Dahlborg, M. Calvo-Dahlborg, P.S. Popel, V.E. Sidorov, Structure and properties of some glass-forming liquid alloys, Eur. Phys. J. B 14 (2000) 639–648.
[52] B.S. Dong, S.X. Zhou, D.R. Li, J.Y. Qin, S.P. Pan, Y.G. Wang, Z.B. Li, Effects of solute-solute avoidance on metallic glass formation, J. Non-Crys. Solids 358 (2012) 2749–2752.
[53] B.S. Dong, S.X. Zhou, J.Y. Qin, S.P. Pan, Z.B. Li, The influence of clusters in the melt of $Fe_{80}Si_{10}B_{10}$ alloy on the subsequent glass-formation, Prog. Nat. Sci. 23 (2013) 216–219.
[54] G.C. Lavorato, G. Fiore, P. Tiberto, M. Baricco, H. Sirkin, J.A. Moya, Structural and magnetic properties of $Fe_{76}P_5(Si_{0.3}B_{0.5}C_{0.2})_{(19)}$ amorphous alloy, J. Alloys Compd. 536 (2012) S319–S323.
[55] G.Y. Zhang, H. Zhang, S.Q. Yue, A.D. Wang, A.N. He, R.J. Cheng, Y.Q. Dong, H.W. Ni, C.-T. Liu, Ultra-low cost and energy-efficient production of FePCSi amorphous alloys with pretreated molten iron from a blast furnace, J. Non-Cryst. Solids 514 (2019) 108–115.
[56] Y.H. Li, Z.M. Wang, W. Zhang, Minor-Cu doped soft magnetic Fe-based FeCoBCSiCu amorphous alloys with high saturation magnetization, AIP Adv. 8 (2018), 056115.
[57] I.W. Donald, H.A. Davies, Prediction of glass-forming ability for metallic systems, J. Non-Cryst. Solids 30 (1978) 77–85.
[58] D. Turnbull, J.C. Fisher, Rate of nucleation in condensed systems, J. Chem. Phys. 17 (1949) 71–73.
[59] A. Kuball, B. Bochtler, O. Gross, V. Pacheco, M. Stolpe, S. Hechler, R. Busch, On the bulk glass formation in the ternary Pd-Ni-S system, Acta Mater. 158 (2018) 13–22.
[60] B.A. Legg, J. Schroers, R. Busch, Thermodynamics, kinetics, and crystallization of $Pt_{57.3}Cu_{14.6}Ni_{5.3}P_{22.8}$ bulk metallic glass, Acta Mater. 55 (2007) 1109–1116.
[61] Y. Li, W.-z. Chen, B.-s. Dong, S.-x. Zhou, Effects of phosphorus and carbon content on the surface tension of FeSiBPC glass-forming alloy melts, J. Non-Cryst. Solids 496 (2018) 13–17.